

ELECTRODYNAMIC STRUCTURE OF OUTER GAP ACCELERATORS: INVISIBILITY OF PULSED TEV FLUXES

K. Hirotani

National Astronomical Observatory, Mitaka, Tokyo 181-8588, Japan; hirotani@hotaka.mtk.nao.ac.jp

ABSTRACT

We study the structure of an outer-magnetospheric gap around a rotating neutron star. Migratory electrons and positrons are accelerated by the electric field exerted in the gap and radiate copious gamma-rays via curvature process. Some of the gamma-rays materialize by colliding with the X-rays illuminating the gap, leading to a pair production cascade. The replenished charges partially screen the original acceleration field, which is self-consistently solved from the Poisson equation, together with the Boltzmann equations for gamma-rays and the continuity equations for particles. We demonstrate that it is difficult to detect the TeV emission due to Compton upscatterings in the gap, by the current ground-based telescopes.

Subject headings: gamma-rays: observation – gamma-rays: theory – magnetic field – X-rays: observation

1. Introduction

In the very high energy (VHE) region above 100 GeV, positive detections of radiation at a high confidence level have been reported from the direction of the Crab, B1706-44, and Vela pulsars (Bowden et al. 1993; Nel et al. 1993; Edwards et al. 1994; Yoshikoshi et al. 1997; see also Kifune 1996 for a review), by virtue of the technique of imaging Cerenkov light from extensive air showers. However, as for *pulsed* TeV radiation, only the upper limits have been obtained from these pulsars. If the VHE emission originates the pulsar magnetosphere, rather than the extended nebula, significant fractions of them are expected to show a pulsation. Therefore, the lack of *pulsed* TeV emissions provides a severe constraint on the modeling of particle acceleration zones in pulsar magnetospheres.

In the picture of Cheng, Ho, and Ruderman (1986a,b), who developed a version of an outer magnetosphere γ -ray emission zone, the magnetosphere should be optically thick for pair production in order that the TeV flux is absorbed to be unobservable. This, in turn, requires very high luminosities of infrared photons, which are generally orders of magnitude larger than the observed values (Usov 1994). We are therefore motivated by the need to contrive an outer gap model which produces less TeV emission with a moderate infrared luminosity.

More recently, Romani (1996) showed that the pulsed TeV flux can be somewhat less than 1% of the pulsed GeV flux, assuming the functional form of the acceleration field as $E_{\parallel} \propto 1/r$, where r denotes the distance from the star. Subsequently, Hirotani (1999, Paper IV) revealed semi-analytically that the TeV fluxes from outer gaps are unobservable, by considering a ‘gap closure condition’ so that a single pair produces copious γ -rays one of which materialize as a pair on average (see also Zhang & Cheng 1998 for another kind of closure condition). In this letter, instead of imposing the closure condition, we investigate the spatial distribution of E_{\parallel} , by solving the Poisson equation and the Boltzmann equations simultaneously. This method was first developed by Beskin et al. (1992) for black-hole magnetospheres and applied to pulsar magnetospheres by Hirotani & Shibata (1999a,b,c; hereafter Paper I, II, III).

We formulate basic equations in § 2, demonstrate the invisibility of pulsed TeV fluxes in § 3, and discuss the validity of assumptions in § 4.

2. Basic Equations and Boundary Conditions

2.1. Reduction of Poisson Equation

To simplify the geometry, let us introduce a rectilinear coordinates for a region around the null surface. Suppose that the magnetic field lines are straight lines parallel to the x axis, where x increases outwardly. We approximate that the null surface ($x = 0$) is perpendicular to the x axis. It is convenient to non-dimensionalize the length scales by a typical Debye scale length c/ω_p (see the discussion in §3.1 in Paper I for details), where

$$\omega_p = \sqrt{\frac{4\pi e^2}{m_e} \frac{\Omega B}{2\pi c e}} = 1.875 \times 10^7 \Omega_2^{1/2} B_5^{1/2} \text{rad s}^{-1}; \quad (1)$$

e refers to the magnitude of the charge on the electron, Ω_2 the angular frequency (Ω) of the neutron star in 10^2rad s^{-1} unit, c the velocity of light, and B_5 the magnetic field strength (B) at $x = 0$ in 10^5 G unit. Then the dimensionless coordinate variable becomes

$$\xi \equiv \frac{\omega_p}{c} x = 6.25 \times 10^{-4} \Omega_2^{1/2} B_5^{1/2} x. \quad (2)$$

Assuming the trans-field thickness is comparable to or greater than the longitudinal width, we Fourier-analyze the Poisson equation in the trans-field directions to obtain (Paper I,II,III)

$$E_{\parallel} = -\frac{d\varphi}{d\xi}, \quad (3)$$

$$\frac{dE_{\parallel}}{d\xi} = -\frac{\varphi}{\Delta_{\perp}^2} + n_+(\xi) - n_-(\xi) - \frac{2\pi c}{\Omega B} \rho_{\text{GJ}}(\xi), \quad (4)$$

where $\Delta_{\perp} \equiv (\omega_p/c) D_{\perp}$ and $\varphi(\xi) \equiv e\Phi(x)/(m_e c^2)$; D_{\perp} is a typical gap thickness in the trans-field directions and Φ the electrostatic potential. The particle densities are normalized in terms of a typical value of the Goldreich–Julian density as

$$n_{\pm}(\xi) \equiv \frac{2\pi c e}{\Omega B} N_{\pm}(x), \quad (5)$$

where $N_{\pm}(x)$ are the spatial number density of e^{\pm} 's. We evaluate it with the Newtonian value as

$$\frac{2\pi c}{\Omega B} \rho_{\text{GJ}} = \frac{2 \cos \theta \cos(\theta - \alpha_i) - \sin \theta \sin(\theta - \alpha_i)}{\sqrt{1 + 3 \cos^2 \theta} [1 - (\varpi/\varpi_{\text{LC}})^2]}, \quad (6)$$

where α_i refers to the inclination angle of the magnetic moment, θ the clatitude angle of the position at which ρ_{GJ} is measured, ϖ the distance from the rotation axis, and $\varpi_{\text{LC}} \equiv c/\Omega$ the light-cylinder radius.

2.2. Boltzmann equations

Let us first introduce the following dimensionless γ -ray densities in the dimensionless energy interval between β_{i-1} and β_i :

$$g_{\pm}^i(\xi) \equiv \frac{2\pi c e}{\Omega B} \int_{\beta_{i-1}}^{\beta_i} d\epsilon_{\gamma} G_{\pm}(x, \epsilon_{\gamma}), \quad (7)$$

where $G_{\pm}(x, \epsilon_{\gamma})$ are the distribution functions of γ -ray photons having momentum $\pm m_e c \epsilon_{\gamma}$. In this letter, we set $\beta_0 = 10$; therefore, the lowest γ -ray energy considered is $10 m_e c^2$. In this letter, we divide the γ -ray spectra into 13 energy bins as follows: $\beta_1 = 30$, $\beta_2 = 100$, $\beta_3 = 200$, $\beta_4 = 300$, $\beta_5 = 600$, $\beta_6 = 10^3$, $\beta_7 = 2 \times 10^3$, $\beta_8 = 3 \times 10^3$, $\beta_9 = 6 \times 10^3$, $\beta_{10} = 10^4$, $\beta_{11} = 2 \times 10^4$, $\beta_{12} = 3 \times 10^4$, $\beta_{13} = 10^5$.

Assuming for simplicity that both electrostatic and curvature-radiation-reaction forces cancel out each other, we obtain the following continuity equations for particles (eqs. [31] and [32] in Paper III):

$$(1 - q) \frac{dn_{\pm}}{d\xi} = \pm \sum_{i=1}^{14} [\eta_{p+}^i g_{+}^i(\xi) + \eta_{p-}^i g_{-}^i(\xi)], \quad (8)$$

$$q \equiv \frac{1}{2} \left(\frac{\pi}{2} \frac{\varpi}{\varpi_{\text{LC}}} \right)^2, \quad (9)$$

The factor $1 - q$ denotes the projection effect due to the three-dimensional motion of the particles, which was not considered in Papers I, II, and III. Since the electric field is assumed to be positive in the gap, e^+ 's (or e^- 's) migrate outwards (or inwards).

The X-ray field affects the gap structure through the pair-production rate $\eta_{p\pm}^i$. Putting $\epsilon_i \equiv (\beta_i + \beta_{i-1})/2$, we can evaluate $\eta_{p\pm}^i$ as

$$\eta_{p\pm}^i = \frac{c}{\omega_p} \int_{\epsilon_{\text{th}}}^{\infty} d\epsilon_x \frac{dN_x}{d\epsilon_x} \sigma_p(\epsilon_i, \epsilon_x, \mu_c), \quad (10)$$

where $dN_x/d\epsilon_x$ denotes the number density of the X-rays between energies ϵ_x and $\epsilon_x + d\epsilon_x$; σ_p is the pair production cross section when two photons collide with an angle $\cos^{-1} \mu_c$ (Berestetskii et al. 1989; eqs. [21]-[23] in Paper II). For surface blackbody X-rays, we obtain $\mu_c = \cos \phi_{\text{abb}} \sin \theta_c$, where $\phi_{\text{abb}} = \tan^{-1}(\varpi/\varpi_{\text{LC}})$ is the aberration angle. For power-law, magnetospheric X-rays, we assume $\mu_c = \cos(0.5W/\varpi_{\text{LC}})$, where W is the full gap width, for both inwardly and outwardly propagating γ -rays. As the lower bound of the integral, the threshold energy, $\epsilon_{\text{th}} \equiv 2(1 - \mu_c)^{-1} \epsilon_{\gamma}^{-1}$, for pair production appears.

A combination of the two continuity equations (8) gives the current density $j_0 \equiv n_+(\xi) + n_-(\xi)$, which is constant for ξ . When $j_0 = 1.0$, the current density equals the typical Goldreich-Julian value, $\Omega B/(2\pi)$.

We next consider the Boltzmann equations for γ -rays. Integrating the γ -ray Boltzmann equations between β_{i-1} and β_i , we obtain (eq. [39] in Paper III)

$$\pm (1 - q) \frac{d}{d\xi} g_{\pm}^i(\xi) = -\eta_{p\pm}^i g_{\pm}^i(\xi) + \eta_c^i n_{\pm}(\xi), \quad (11)$$

where $i = 1, 2, \dots, m (= 13)$. The γ -ray production rate via curvature radiation, η_c^i , are defined by equation (40) in Paper III. The particle motion is assumed to be mono-energetic and the Lorentz factor saturates in a balance between electrostatic acceleration and the curvature drag force (see eq. [19] in Paper III).

2.3. Boundary Conditions

In the same manner as in Papers I, II, and III, we impose the boundary conditions at the inner ($\xi = \xi_1$) and outer ($\xi = \xi_2$) boundaries as follows:

$$E_{\parallel}(\xi_1) = 0, \quad \varphi(\xi_1) = 0, \quad (12)$$

$$g_{+}^i(\xi_1) = 0, \quad n_{+}(\xi_1) = 0, \quad n_{-}(\xi_1) = j_0, \quad (13)$$

$$E_{\parallel}(\xi_2) = 0, \quad g_{-}^i(\xi_2) = 0, \quad n_{-}(\xi_2) = 0, \quad (14)$$

where $i = 1, 2, \dots, m$. We have totally $2m + 6$ boundary conditions (12)–(14) for $2m + 4$ unknown functions Φ , E_{\parallel} , n_{\pm} , $g_{\pm}^1 \dots g_{\pm}^m$. Thus two extra boundary conditions must be compensated by making the positions of the boundaries ξ_1 and ξ_2 be free. The two free boundaries appear because $E_{\parallel} = 0$ is imposed at the *both* boundaries and because j_0 is externally imposed.

2.4. TeV Fluxes

The pair production cascade is primarily described by the curvature-radiated, GeV γ -rays. Therefore, the TeV emission due to Compton upscatterings is energetically negligible and can be computed passively from the electrodynamic structure of the gap. Assuming that the azimuthal gap width is $0.5\pi W/\varpi_{\text{LC}} (\equiv h)$ rad, we can evaluate the ratio between the TeV flux and the infrared one as (see §2.7 in Paper V)

$$f_{\text{R}} \equiv \frac{(\nu F_{\nu})_{\text{TeV}}}{(\nu F_{\nu})_{0.1\text{eV}}} < 5.63 \times 10^{-5} \left(\frac{\varpi_{\text{LC}}}{r_0} \sin \theta_0 \right) \times \Gamma \left(j_0 \frac{D_{\perp}}{\varpi_{\text{LC}}} \right) B_5 \frac{\omega_{0.1\text{eV}}}{\omega_{\text{TeV}}} h^2, \quad (15)$$

where ω_E refers to the solid angle in which photons with energy E are emitted; $\omega_{\text{TeV}} = \omega_{0.1\text{eV}}$ is assumed for simplicity. To estimate the upper bound, we take $D_{\perp} = \varpi_{\text{LC}}$. The inequality comes from the fact that the scattered photon energy cannot exceed the particle energy. It is noteworthy that it is the infrared photons with energy ~ 0.1 eV that contribute most effectively as the target photons of comptonization. Neither the higher energy photons like surface blackbody X-rays nor the lower energy photons like polar-cap radio emission contribute as the target photons, because they have either too small cross sections or too small energy transfer when they are scattered.

Substituting the X-ray fields, Ω and μ of individual pulsars into the differential equations, we can solve $E_{\parallel}(\xi)$ and hence h ; equation (15) then gives f_{R} as a function of α_i and j_0 .

3. Application to Individual Pulsars

In this section, we apply the theory to seven rotation-powered pulsars. We first present the observed X-ray properties of individual pulsars as input parameters in order of spin-down luminosity in table 1. The X-ray spectrum of each pulsar is approximated by separating into a soft blackbody component with temperature kT_s and emitting area A_s , a hard blackbody one with kT_h and A_h , and a power-law one with $dN_x/d\epsilon_x = N_{\text{pl}}\epsilon_x^{\alpha}$ ($\epsilon_{\text{min}} < \epsilon_x < \epsilon_{\text{max}}$), where $\epsilon_{\text{min}} = 0.1\text{keV}/511\text{keV}$ and $\epsilon_{\text{max}} = 50\text{keV}/511\text{keV}$ are assumed for homogeneous discussion.

Let us next consider the TeV fluxes. As a typical example, we present the results of f_{R} for B1509-58 as a function of α_i and j_0 in figure 1. The filled circles correspond to the maximum current density j_{cr} above which no solution exists (see § 3.1 in Paper III and § 3.1 in Hirofani & Okamoto 1998 for details) if all the other parameters are fixed. It follows from the figure that f_{R} becomes maximum at $j_0 = j_{\text{cr}}$ (for a given α_i). We thus consider the case of $j_0 = j_{\text{cr}}$ in this section to estimate the upper bound of f_{R} .

The upper bound of f_{R} for the seven pulsars are presented in table 2. For Crab and B0540-69, the synchrotron (or synchro-curvature) process dominates the simple curvature one when $\alpha_i = 60^\circ$; therefore, this case is excluded in the table. For B1055-52, acceleration length scale for a particle to attain the saturated Lorentz factor exceeds the gap half width for $\alpha_i = 60^\circ$. In another word, the mono-energetic approximation breaks down; therefore, the case of

$\alpha_i = 60^\circ$ is excluded. It follows from the table that the TeV fluxes are unobservable ($< 10^{12}$ Jy Hz) for moderate infrared fluxes ($< 10^9$ Jy Hz), even when j_0 is adjusted close to j_{cr} .

4. Discussion

In summary, we have developed a one-dimensional model for an outer-gap accelerator. As the inclination angle (α_i) increases, the gap center (where B_z vanishes) shifts starwards to be illuminated by a strong X-ray field, which reduces the pair production mean free path and hence the gap longitudinal width, W . At the same time, the starwardly shifted gap has a strong magnetic field, which increases the acceleration field (see eq. [4]). As a result, the TeV flux increases with increasing α_i , even though W decreases. However, it is difficult to detect the TeV flux, even when α_i is as large as 60° . We can therefore conclude that the difficulty of excessive TeV emission, which appears in the picture of Cheng, Ho, and Ruderman (1986a,b), does not arise in the present outer gap model.

It is seemingly possible to obtain observable TeV fluxes, if α_i exceeds 60° . In this case, the ‘outer gap’ is located close to the polar cap; the distance from the star is within 13% of ϖ_{LC} . The magnetic field there is so strong that the synchrotron (or synchro-curvature) process becomes important in general; this could be verified by computing the pitch angle evolution of particles created in the gap (see §5.3 in Paper I). Such a ‘polar-gap-like’ outer gap will be discussed in a separate paper.

For middle-age pulsars B0656+14 and Geminga, there is no stationary solution that satisfies the boundary conditions presented in §2.3. However, if we allow an external electric current flowing into the gap at the outer boundary, there exists a branch of solutions. In this case, the gap is no longer located around the null surface but shifts starwards. Interestingly, when the external current density approaches the Goldreich-Julian value, the ‘outer gap’ is found to shift to the polar cap and have a similar electrodynamic structure of Scharlemann, Arons, & Fawley (1978). Such a unification of the outer gap and polar cap accelerators will be discussed in separate papers.

This research owes much to the helpful comments of Dr. S. Shibata. The author wishes to express his gratitude to Drs. Y. Saito and A. Harding for valu-

Table 1: Input parameters and X-ray fields

pulsar	distance kpc	Ω rad s $^{-1}$	$\log_{10} \mu$ lg(G cm 3)	kT_s keV	A_s/A_*^\dagger	kT_h keV	A_h/A_*^\dagger	N_{pl} cm $^{-3}$	$-\alpha$	ref.
Crab	2.49	188.1	30.53	$10^{17.30}$	1.8	1
B0540-69	49.4	124.7	31.00	$10^{14.15}$	2.0	2
B1509-58	4.40	41.7	31.19	$10^{14.04}$	1.1	2
J1617-5055	3.30	90.6	30.78	$10^{12.64}$	1.6	3,4
Vela	0.50	61.3	30.53	150	0.066	5
B1951+32	2.5	159	29.68	$10^{13.55}$	1.6	6
B1055-52	1.53	31.9	30.03	68	7.3	320	$10^{-3.64}$	7

$^\dagger A_* = 4\pi r_*^2$ represents the whole neutron star surface area; $r_* = 10$ km is assumed.

References: 1 Knight (1982) 2 Saito (1998) 3 Torii et al. (1998) 4 Caswell et al. (1975)

5 Ögelman et al. (1993) 6 Safi-Harb and Ögelman (1995) 7 Greiveldinger et al. (1996)

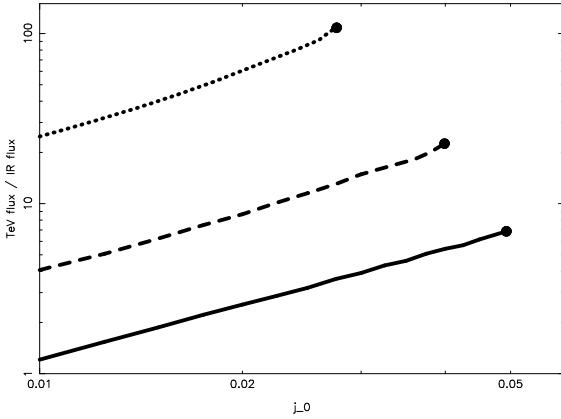


Fig. 1.— $f_R \equiv (\nu F_\nu)_{\text{TeV}} / (\nu F_\nu)_{0.1\text{eV}}$ vs. j_0 for B1509-58, where $(\nu F_\nu)_E$ indicates the νF_ν flux at photon energy E . The solid, dashed, and dotted lines correspond to $\alpha_i = 30^\circ$, 45° , and 60° , respectively.

 Table 2: Expected γ -ray properties

pulsar	α_i deg	$j_0 = j_{\text{cr}}$	$W/\varpi_{\text{LC}}^\dagger$	f_R^\ddagger
Crab	30	0.0485	0.083	6.1×10^1
	45	0.0371	0.064	1.8×10^2
B0540-69	30	0.0390	0.074	4.2×10^1
	45	0.0305	0.053	1.2×10^2
B1509-58	30	0.0375	0.102	5.1×10^0
	45	0.0399	0.083	2.3×10^1
	60	0.0276	0.052	1.1×10^2
J1617-5055	30	0.0627	0.136	4.5×10^1
	45	0.0430	0.104	1.2×10^2
	60	0.0241	0.049	3.2×10^2
Vela	30	0.0620	0.255	2.8×10^1
	45	0.0375	0.142	4.2×10^1
B1951+32	60	0.0264	0.085	1.7×10^2
	30	0.0450	0.133	1.2×10^1
	45	0.0380	0.095	3.7×10^1
B1055-52	60	0.0272	0.057	1.8×10^2
	30	0.0343	0.443	2.1×10^0
	45	0.0232	0.182	1.6×10^0

$^\dagger W$ indicates the full gap width.

$^\ddagger f_R \equiv (\nu F_\nu)_{\text{TeV}} / (\nu F_\nu)_{0.1\text{eV}}$.

able advice. He also thanks the Astronomical Data Analysis Center of National Astronomical Observatory, Japan for the use of workstations.

REFERENCES

- Berestetskii, V. B., Lifshitz, E. M. & Pitaevskii, L. P., 1989, *Quantum Electrodynamics* 3rd ed.
- Beskin, V. S., Istomin, Ya. N., & Par'ev, V. I. 1992, *Sov. Astron.* 36(6), 642
- Bowden, C. C. G. et al. 1993, *Proc. of 23rd Int. Cosmic Ray Conf. (Calgary)*, 1, 294
- Caswell, J. L., Murray, J. D., Roger, R. S., Cole, D. J., Cooke, D. J. 1975, *A& A* 45, 239
- Cheng, K. S., Ho, C., Ruderman, M., 1986a *ApJ*, 300, 500
- Cheng, K. S., Ho, C., Ruderman, M., 1986b *ApJ*, 300, 522
- Edwards, P. G., et al. 1994 *A& A* 291, 468
- Greiveldinger, C. et al. 1996, *ApJ* 465, L35
- Hirovani, K. 1999 (Paper IV), submitted to *ApJ*
- Hirovani, K. Okamoto, I. 1998, *ApJ* 497, 563
- Hirovani, K. Shibata, S., 1999a (Paper I), *MNRAS* 308, 54
- Hirovani, K. Shibata, S., 1999b (Paper II), *MNRAS* 308, 76
- Hirovani, K. Shibata, S., 1999c (Paper III), *PASJ* 51, 683
- Kifune, T. 1996, *Space Science Reviews* 75, 31
- Knight F. K. 1982, *ApJ* 260, 538
- Nel, H. I. et al. 1993, *ApJ* 418, 836
- Ögelman, H., Finley, J. P., Zimmermann, H. U. 1993, *Nature* 361, 136
- Romani, R. W. 1996, *ApJ*, 470, 469
- Safi-Harb, S. Ögelman, H. 1995, *ApJ* 439, 722
- Safi-Harb, S. Ögelman, H. 1995, *ApJ* 439, 722
- Saito, Y. 1998, Ph.D. Thesis
- Scharlemann, E. T., Arons, J., & Fawley, W. M. 1978, *ApJ*, 222, 297
- Torii, K. et al. 1998, *ApJ* 494, L207
- Usov, V. V. 1994, *ApJ* 427, 394
- Yoshikoshi, T., et al. 1997, *ApJ* 487, L65
- Zhang, L. Cheng, K. S. 1998, *MNRAS* 294, 177